INSTITUTE OF PHYSICS PUBLISHING JOURNAL OF PHYSICS: CONDENSED MATTER

J. Phys.: Condens. Matter **15** (2003) 8315–8326 PII: S0953-8984(03)66393-9

Cation-size control of structural phase transitions in tin perovskites

Elizabeth H Mountstevens[1,2], J Paul Attfield[2] and Simon A T Redfern[1]

[1] Department of Earth Sciences, University of Cambridge, Downing Street, Cambridge CB2 3EQ, UK
[2] Department of Chemistry, University of Cambridge, Lensfield Road, Cambridge CB2 1EW, UK

Received 18 July 2003
Published 25 November 2003
Online at stacks.iop.org/JPhysCM/15/8315

Abstract

The structural evolution at 300 K of the series $Sr_xBa_{1-x}SnO_3$ and $Sr_xCa_{1-x}SnO_3$ at $x = 0.2$ intervals has been determined by powder neutron diffraction. All $Sr_xCa_{1-x}SnO_3$ samples ($x = 0$–1) have the $Pbnm$ superstructure. In the series $Sr_xBa_{1-x}SnO_3$, the $x = 1.0$ and 0.8 samples have the $Pbnm$ superstructure. The $x = 0.6$ sample has a second orthorhombic structure with space group $Imma$. There is a tetragonal $I4/mcm$ phase at $x = 0.4$ and the undistorted cubic $Pm\bar{3}m$ structure for $x = 0.2$ and $BaSnO_3$. The octahedral tilt angles show a smooth variation with average A cation radius over the range of superstructures described by mean field theory close to the transition. The transitions are also analysed via the variation of spontaneous strains.

1. Introduction

The alkaline earth stannates, $ASnO_3$ (A = Ca, Sr, Ba), have recently been investigated as potential capacitor components with a small temperature coefficient of capacitance [1]. Stannates form solid solutions with barium titanate and when added in small quantities will lower the temperature of the ferroelectric transition [2]. $SrSnO_3$ has been studied as a high temperature humidity sensor and is especially effective when doped with La^{3+} [3]. Recently there has also been interest in the alkaline earth stannates as nitrogen oxide absorbers in lean exhaust gases [4]. The nitrogen oxide gases are trapped on a selective adsorbent such as the stannates and then reduced using a small burst of fuel or recirculated to the engine to be thermally destroyed. $BaSnO_3$ shows particular promise as a selective adsorbant.

All of the alkaline earth stannates have perovskite structures. $CaSnO_3$ is orthorhombic at room temperature with the common $\sqrt{2}a \times \sqrt{2}a \times 2a$ $Pbnm$ superstructure of the ideal perovskite cell (cubic parameter a) [5]. $SrSnO_3$ was originally thought to have a doubled cubic structure with 8 formula units per unit cell [6]. More recently, however, powder neutron diffraction has shown $SrSnO_3$ also to have the orthorhombic $Pbnm$ structure [7]. $BaSnO_3$

has the simple cubic $Pm\bar{3}m$ perovskite structure [8]. Sn^{4+} is similar in size to Ti^{4+} and other transition metal ions but has no off-centre, Jahn–Teller, or other electronically driven distortions. The alkaline earth stannates therefore give good insights into the evolution of the perovskite structure by octahedral tilting and deformation on substitution at the A site.

Stannate perovskites also provide a good analogue to magnesium silicate perovskites which are believed to be the main constituent of the Earth's lower mantle. Detailed investigations on $MgSiO_3$ perovskite are difficult due to the instability of this phase at ambient temperatures and pressures. In particular, high temperature studies at low pressure are precluded by the breakdown of $MgSiO_3$. Furthermore, $MgSiO_3$ is usually synthesized only in very small quantities (of the order of milligrams). Germanate perovskites might be considered a good analogue of the silicate perovskites but Andrault and co-workers [9] showed that these phases exist only metastably at ambient pressure and temperature, amorphizing upon heating. Stannate perovskites, on the other hand, are stable under ambient conditions and tin is in the same group as silicon. Stannates may therefore be able to provide useful information about the structural chemistry of silicate perovskites.

The solid solutions $Sr_xBa_{1-x}SnO_3$ and $Sr_xCa_{1-x}SnO_3$ were first studied by Smith and Welch [6] in 1960. They observed a transition from the cubic $BaSnO_3$ structure to the doubled cubic $SrSnO_3$ structure at 80 mol% strontium. In the $Sr_xCa_{1-x}SnO_3$ solid solution, a transition from the doubled cubic $SrSnO_3$ structure to the orthorhombic $CaSnO_3$ structure was observed at 45 mol% strontium. We have reexamined these solid solutions in light of the new structural information on $SrSnO_3$ [7].

2. Experimental details

Samples were prepared by mixing stoichiometric quantities of $BaCO_3$, $SrCO_3$, $CaCO_3$ and SnO_2. The powders were ground together using an agate pestle and mortar and pressed into 13 mm diameter pellets under a load of 9 tons. These pellets were fired in air at temperatures between 1360 and 1400 °C for 24 h and furnace cooled to room temperature over a period of 2 h. The solid solution samples were reground and refired a further two times using the same method. Powder x-ray diffraction showed that all samples appeared to be a single perovskite phase.

High-resolution room temperature powder neutron diffraction patterns were collected using the D2B diffractometer at the Institute Laue Langevin (ILL), Grenoble. The thermal beam of neutrons is monochromated using a germanium crystal to give a wavelength of 1.5943 Å. Data were collected in the range $2\theta = 4$–$160°$ in 0.025° steps for 4 h.

Fitting of the diffraction patterns was performed by the Rietveld method using the general structure analysis system (GSAS) software package [10]. The data sets were fitted using a linear background function and a pseudo-Voigt peak shape. Background coefficients, diffractometer zero, lattice parameters, isotropic temperature factors, atomic positions and profile coefficients were refined.

No impurity phases were detected in any of the neutron profiles and initially all samples were refined as single phases, but this gave a poor fit for the $Sr_xCa_{1-x}SnO_3$ solid solutions and the peaks were seen to be slightly split, suggesting a slight inhomogeneity in the samples. The refinements were repeated fitting two perovskite phases with the same symmetry. Atomic positions and isotropic temperature factors were constrained to be the same for the two phases while lattice parameters and phase fractions were allowed to vary independently. This gave a much better fit to the data; for example, for $Sr_{0.6}Ca_{0.4}SnO_3$, the χ^2-value reduced from 23.57 to 1.74. The samples in the solid solution $Sr_xBa_{1-x}SnO_3$ were also refined as two phases for consistency, although this only produced a significant decrease in χ^2 for $Sr_{0.4}Ba_{0.6}SnO_3$.

Table 1. Refinement results for $BaSnO_3$, $SrSnO_3$, $CaSnO_3$. For each sample the space group, lattice parameters, atomic positions and isotropic temperature factors are listed as well as R-factors and χ^2-values for the fit.

Atom	x	y	z	$100U_{ISO}$ (Å^2)
$BaSnO_3$ $Pm\bar{3}m$ $a = 4.1151(1)$ Å				
A	0.5	0.5	0.5	0.35(2)
Sn	0.0	0.0	0.0	0.20(2)
O	0.5	0.0	0.0	0.71(1)
$R_P = 5.03\%$ $wR_P = 6.28\%$ $R(F^2) = 1.59\%$ $\chi^2 = 1.58$				
$SrSnO_3$ $Pbnm$ $a = 5.7079(2)$ Å, $b = 5.7035(2)$ Å, $c = 8.0645(2)$ Å				
A	−0.0062(5)	0.0193(2)	0.25	0.80(2)
Sn	0.0	0.5	0.0	0.09(2)
O1	0.0601(4)	0.4921(2)	0.25	0.74(3)
O2	0.7184(2)	0.2802(2)	0.0325(2)	0.74(2)
$R_P = 4.43\%$ $wR_P = 5.80\%$ $R(F^2) = 2.91\%$ $\chi^2 = 3.15$				
$CaSnO_3$ $Pbnm$ $a = 5.5142(2)$ Å, $b = 5.6620(2)$ Å, $c = 7.8814(2)$ Å				
A	−0.0141(3)	0.0506(2)	0.25	0.82(3)
Sn	0.0	0.5	0.0	0.14(2)
O1	0.0997(2)	0.04644(2)	0.25	0.52(2)
O2	0.6988(1)	0.2982(1)	0.0517(1)	0.54(2)
$R_P = 4.42\%$ $wR_P = 5.49\%$ $R(F^2) = 3.56\%$ $\chi^2 = 2.35$				

Weighted averages of the cell parameters were used in the subsequent analyses of strains, bond distances, etc for the samples fitted by two phases.

3. Results

As reported previously, $BaSnO_3$ has the undistorted cubic perovskite structure with space group $Pm\bar{3}m$, whereas $SrSnO_3$ and $CaSnO_3$ are orthorhombic with space group $Pbnm$. The $Pbnm$ superstructure involves in-phase tilting of SnO_6 octahedra about the c-axis and out-of-phase tilting about the diad axis parallel to the b-axis. The structural, atomic and thermal parameters for the end members are given in table 1 and are in general agreement with those from the previous studies [5–8].

All members of the $Sr_xCa_{1-x}SnO_3$ solid solution have space group $Pbnm$. The structural, atomic and thermal parameters for these samples are listed in table 2. Figure 1 shows the observed, calculated and difference diffraction pattern of $Sr_{0.4}Ca_{0.6}SnO_3$, the sample with the most extreme inhomogeneity.

The barium-rich end of $Sr_xBa_{1-x}SnO_3$ is cubic and $x = 0.0$ and 0.2 have the $Pm\bar{3}m$ structure at 300 K, with no superlattice reflections in the diffraction patterns (figure 2). $Sr_{0.4}Ba_{0.6}SnO_3$ has a tetragonal superstructure, space group $I4/mcm$, with out-of-phase tilting of octahedra about the c-axis. The diffraction pattern exhibits reflections due to R-point, $k = (1/2, 1/2, 1/2)$, distortions but no reflections due to M-point, $k = (1/2, 1/2, 0)$, distortions, as can be seen from figure 2. The R-point distortions correspond to out-of-phase tilting of whereas the M-point distortions result in in-phase tilting [11]. A third type of distortion created by tilting of the octahedra are X-point, $k = (0, 0, 1)$, distortions which occur when R-point and M-point distortions operate in concert.

$Sr_{0.6}Ba_{0.4}SnO_3$ also exhibits R-point reflections but not M-point reflections (figure 2); however at high 2θ angles there is an additional splitting that is not consistent with tetragonal

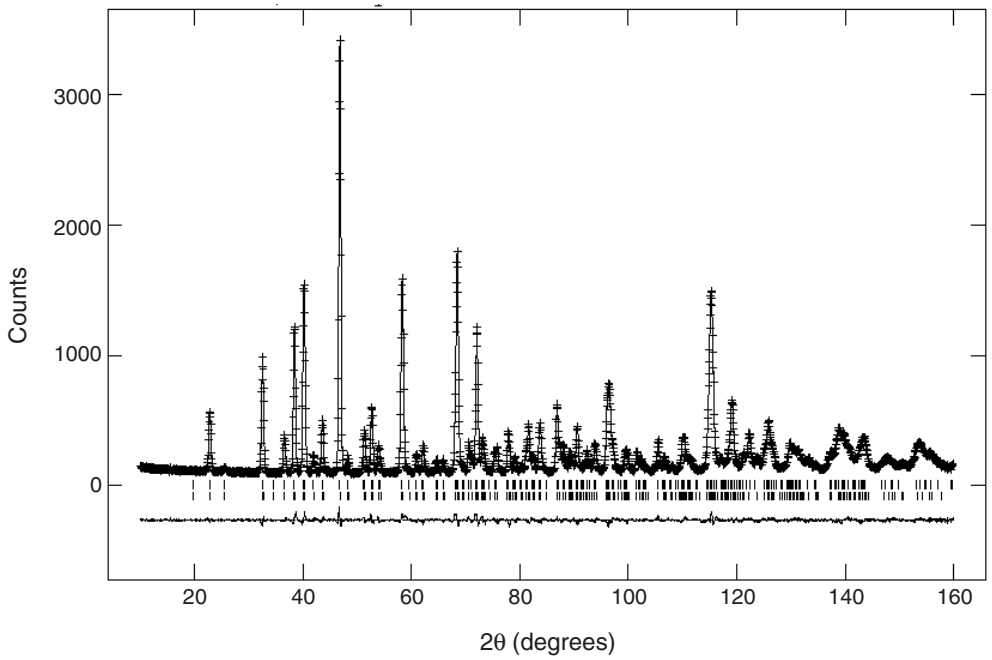

Figure 1. Observed, calculated and difference powder neutron diffraction profiles for $Sr_{0.4}Ca_{0.6}SnO_3$ with reflection markers for the two fitted *Pbnm* phases.

symmetry. This sample has the space group *Imma* which describes out-of-phase tilting about the diad axis parallel to the *b*-axis. This space group accounted for this additional splitting and all the other reflections present as illustrated in figure 3. A two-phase $Imma + I4/mcm$ region was reported in the $Ba_{1-x}Sr_xZrO_3$ solid solution [12], however, it was not possible to establish whether this occurs in the $Sr_xBa_{1-x}SnO_3$ system because of the small sample inhomogeneities.

The solid solution $Sr_xBa_{1-x}SnO_3$ has the orthorhombic *Pbnm* structure at the strontium-rich end ($x = 1.0$ and 0.8). The diffraction patterns are characterized by the appearance of superlattice reflections due to both R-point and M-point distortions (see figure 2). The presence of both distortions leads to additional X-point distortions [11].

The structural, atomic and positional parameters for the $Sr_xBa_{1-x}SnO_3$ samples are given in table 3. The variation of pseudocubic cell volume and pseudocubic lattice parameters with average A cation size are shown in figures 4 and 5. Figure 6 shows the variation of average Sn–O bond length with average radius of A cation.

Figure 7 shows the variation in tilt angle with average radius of the A cation. Perovskite structures typically distort by tilting of the octahedra. Octahedra in adjacent unit cells may tilt in the same sense (in-phase tilting, ϕ_+) or in the opposite sense (out-of-phase tilting, ϕ_-). The tilt angles may be estimated from cell parameters, although this assumes that the octahedra are undistorted. We have calculated the tilt angles from the following oxygen atomic positions using the method of Kennedy *et al* [13]:

Pbnm	O2	$(1/2 - u, 1/2 + v, w)$	$\tan\phi_+ = 2(u + v)$	$\tan\phi_- = 4\sqrt{2}w$
Imma	O2	$(1/2, v, 1/2)$	$\tan\phi_- = 4\sqrt{2}v$	
$I4/mcm$	O2	$(1/2 + u, 1/2 + u, 0)$	$\tan\phi_- = 4u$.	

Table 2. Refinement results for $Sr_xCa_{1-x}SnO_3$ as in table 1. The standard deviations in the lattice parameters are calculated from the distribution of the two values produced by the two phase fits.

Atom	x	y	z	$100U_{ISO}$ (Å^2)
$x = 0.2$ $Pbnm$ $a = 5.557(16)$ Å, $b = 5.667(4)$ Å, $c = 7.924(15)$ Å				
A	−0.0133(4)	0.0432(2)	0.25	0.68(3)
Sn	0.0	0.5	0.0	0.28(2)
O1	0.0922(3)	0.4700(2)	0.25	1.01(3)
O2	0.7011(2)	0.2952(2)	0.0480(1)	0.93(3)
$R_P = 3.89\%$ $wR_P = 4.78\%$ $R(F^2) = 3.66\%$ $\chi^2 = 2.08$				
$x = 0.4$ $Pbnm$ $a = 5.599(17)$ Å, $b = 5.674(1)$ Å, $c = 7.979(9)$ Å				
A	−0.0121(5)	0.0373(2)	0.25	1.07(3)
Sn	0.0	0.5	0.0	0.19(2)
O1	0.0859(4)	0.4757(3)	0.25	0.86(4)
O2	0.7044(2)	0.2921(2)	0.0429(2)	0.81(3)
$R_P = 3.94\%$ $wR_P = 4.86\%$ $R(F^2) = 4.18\%$ $\chi^2 = 2.41$				
$x = 0.6$ $Pbnm$ $a = 5.642(7)$ Å, $b = 5.6822(2)$ Å, $c = 8.005(2)$ Å				
A	−0.0087(4)	0.0329(2)	0.25	0.89(3)
Sn	0.0	0.5	0.0	0.21(2)
O1	0.0782(3)	0.4806(2)	0.25	0.91(3)
O2	0.7097(2)	0.2892(2)	0.0394(1)	0.89(2)
$R_P = 3.25\%$ $wR_P = 3.87\%$ $R(F^2) = 2.92\%$ $\chi^2 = 1.74$				
$x = 0.8$ $Pbnm$ $a = 5.675(1)$ Å, $b = 5.691(2)$ Å, $c = 8.032(1)$ Å				
A	−0.051(4)	0.0271(2)	0.25	0.78(2)
Sn	0.0	0.5	0.0	0.18(2)
O1	0.0720(4)	0.4861(3)	0.25	0.81(3)
O2	0.7147(2)	0.2849(2)	0.0352(2)	0.81(2)
$R_P = 3.67\%$ $wR_P = 4.43\%$ $R(F^2) = 3.62\%$ $\chi^2 = 2.03$				

The variation of tilt angles with average radius of the A cation are described well by a critical equation: $\phi_{+/-} = \phi_{+/-}(0)(1 - r/r_c)^\beta$. For the in-phase tilting, the fitted parameters are $\phi_+(0) = 33(1)^\circ$, $r_c = 1.498(3)$ Å and $\beta = 0.47(2)$. β is close to 0.5, the value expected for a second-order transition in mean field theory. For out-of-phase tilting, β was fixed at 0.5 to give a stable fit, giving $\phi_-(0) = 40(2)^\circ$ and $r_c = 1.556(5)$ Å. The r_c-values define the $Pbnm$ to $Imma$ and $I4/mcm$ to $Pm\bar{3}m$ structural phase boundaries.

An alternative to the octahedral tilting description of the evolution of phase transitions in perovskites is to describe the transformations in terms of spontaneous strains using the language of ferroelastic phase transitions. Spontaneous strains in stannates are the macroscopic averages of rotations and distortions of individual SnO_6 octahedra. We have carried out such a strain analysis using the method of Carpenter *et al* [14]. A baseline to the paraphase cell parameters was found by fitting a second-order polynomial to the cube root of the volume. The spontaneous strains were calculated from the lattice parameters as follows.

$$Pm\bar{3}m: \qquad e = 0$$

$$I4/mcm: \qquad e_1 = e_2 = \frac{a}{\sqrt{2}a_0} - 1 \qquad e_3 = \frac{c}{2a_0} - 1$$

$$Imma: \qquad e_1 = \frac{c}{\sqrt{2}a_0} - 1 \qquad e_2 = \frac{b}{2a_0} - 1 \qquad e_3 = \frac{a}{\sqrt{2}a_0} - 1$$

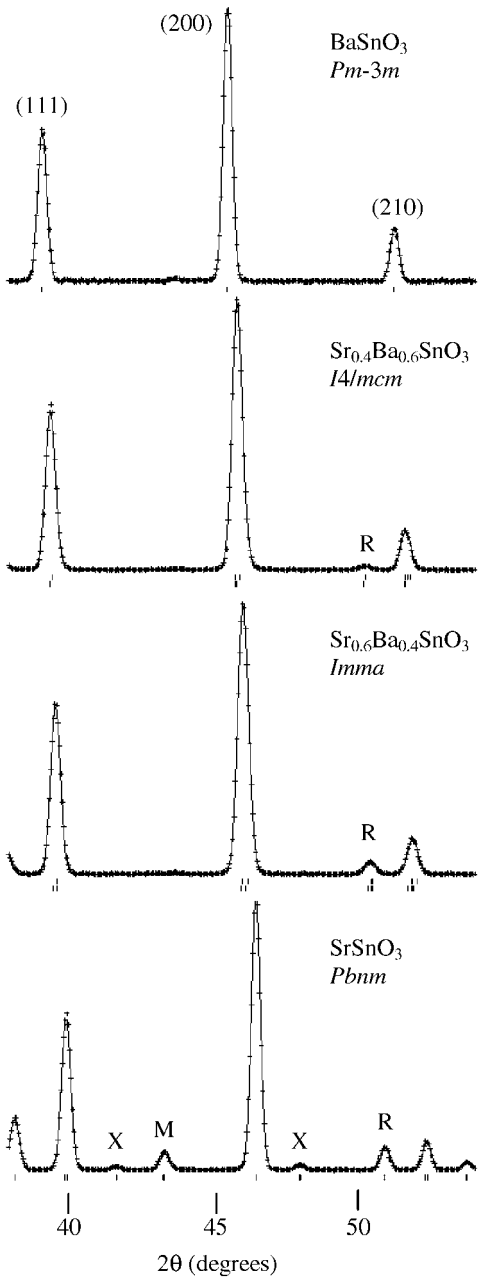

Figure 2. Observed and calculated powder neutron diffraction profiles for $Sr_xBa_{1-x}SnO_3$ for $x = 0.0$, 0.4, 0.6 and 1.0 in the range $38° < 2\theta < 54°$. Superstructure reflections produced by R-, M- and X-point distortions are indicated.

$$Pbnm: \qquad e_1 = \frac{b}{\sqrt{2}a_0} - 1 \qquad e_2 = \frac{a}{\sqrt{2}a_0} - 1 \qquad e_3 = \frac{c}{2a_0} - 1.$$

The spontaneous strains were combined to give symmetry-adapted strains which are the volume

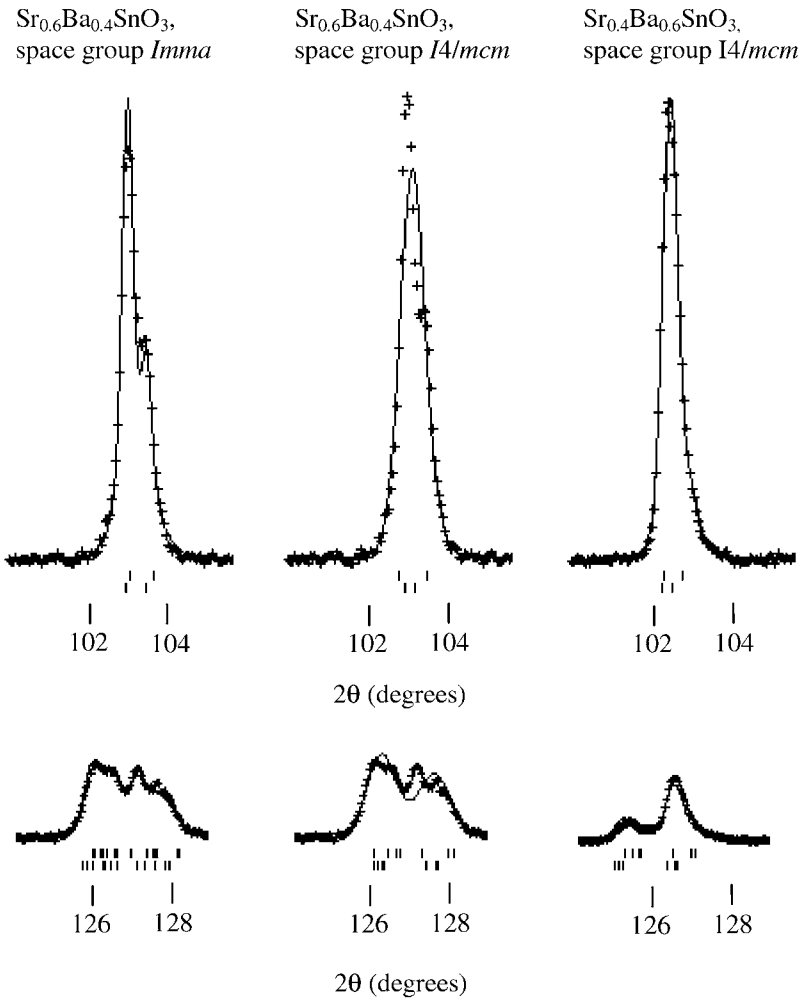

Figure 3. Observed and calculated powder neutron diffraction profiles for two sets of high-angle reflections for $Sr_{0.6}Ba_{0.4}SnO_3$ and $Sr_{0.4}Ba_{0.6}SnO_3$, showing how the fit to the former data is improved when the symmetry is lowered from tetragonal $I4/mcm$ to orthorhombic $Imma$.

strain (e_a), the tetragonal strain (e_t), and the orthorhombic (e_o) strain:

$$e_a = e_1 + e_2 + e_3$$
$$e_t = \frac{1}{\sqrt{3}}(2e_3 - e_1 - e_2)$$
$$e_o = e_1 - e_2.$$

The variations of symmetry-adapted strains with average A cation radius are shown in figure 8.

4. Discussion

The chemical variation of $ASnO_3$ superstructures with increasing A cation radius at 300 K has been determined through these powder neutron diffraction experiments. Both the cell volume (figure 4) and the lattice parameters (figure 5) increase with increasing A cation size,

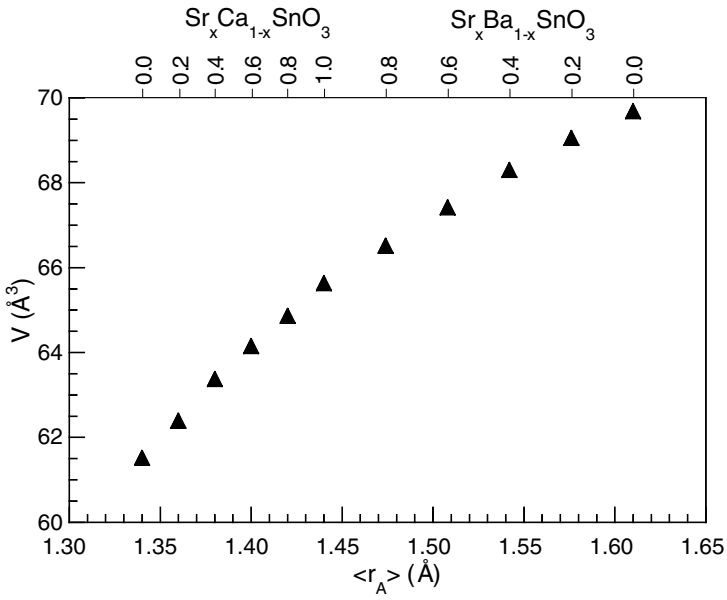

Figure 4. Variation of pseudocubic unit cell volume with average A cation radius of $ASnO_3$ perovskites.

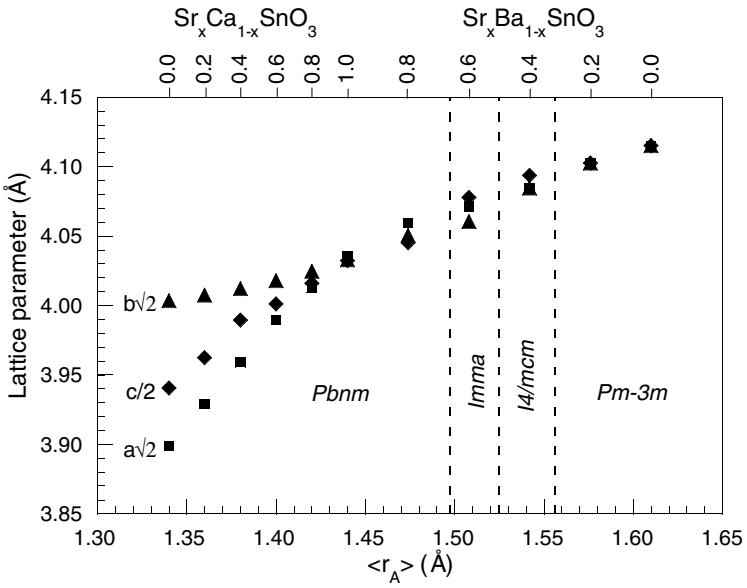

Figure 5. Variation of pseudocubic lattice parameters with average A cation radius.

as expected. The average Sn–O bond length (figure 6) does not change monotonically with cation radius, but instead shows a minimum close to the tetragonal–orthorhombic boundary. We propose that this is an artefact of crystallographic averaging over locally bent Sn–O–Sn bridges. At tolerance factor $t = 1$, the local (and cubic $Pm\bar{3}m$ average) Sn–O–Sn angles are 180°. As t initially decreases below $t = 1$, the Sn–O–Sn bridges start to bend locally, but their

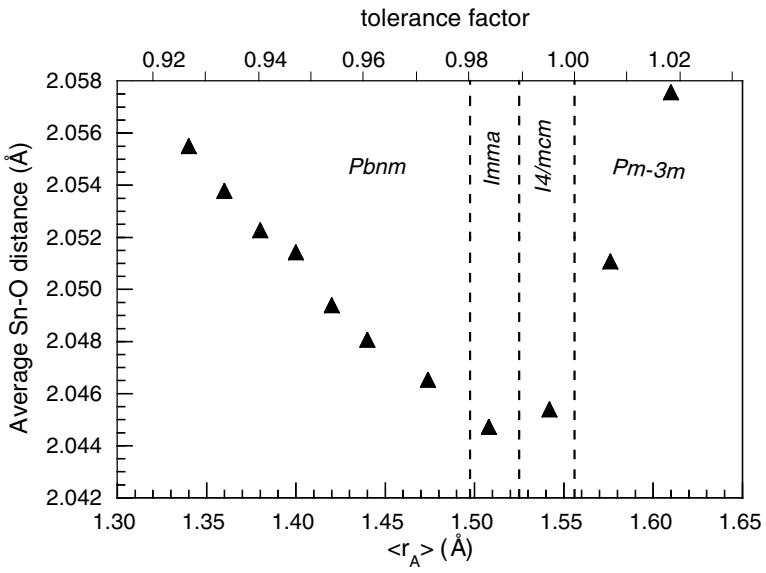

Figure 6. Variation of average Sn–O bond length with average radius of A cation and the perovskite tolerance factor.

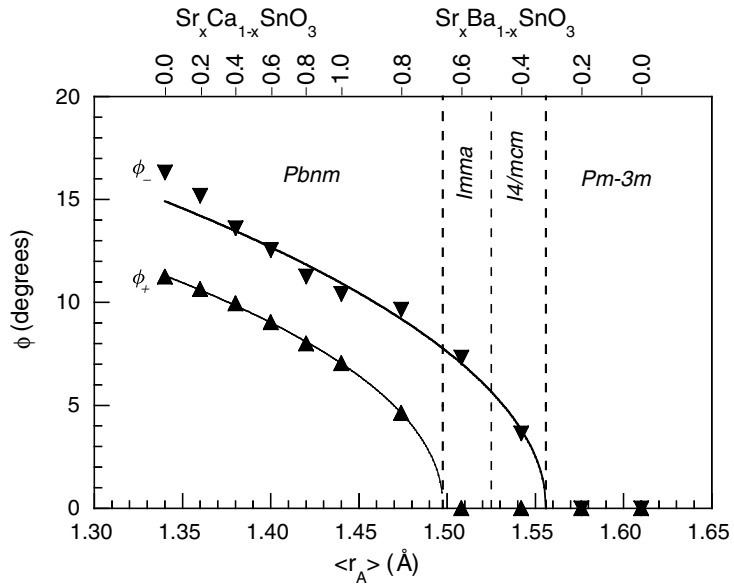

Figure 7. Variation of rotation angle with average radius of A cation for in-phase tilting, ϕ_+, and out-of-phase tilting of octahedra, ϕ_-. The fitted curves are given by the critical equation: $\phi_{+/-} = \phi_{+/-}(0)(1 - r/r_c)^{\beta}$.

average is still linear in the $Pm\bar{3}m$ and (for some bridges) in the tetragonal $I4/mcm$ space groups, so the apparent average Sn–O distance decreases as t decreases. At the $I4/mcm$ to $Imma$ transition, the bending of all Sn–O–Sn bonds becomes structurally coherent (i.e. all crystallographic average bond angles are $<180°$), and as the structural coherence increases

Table 3. Refinement results for $Sr_xBa_{1-x}SnO_3$ as in tables 1 and 2.

Atom	x	y	z	$100U_{ISO}$ (Å^2)
	$x = 0.2$ $Pm\bar{3}m$ $a = 4.102(2)$ Å			
A	0.5	0.5	0.5	0.59(2)
Sn	0.0	0.0	0.0	0.25(2)
O	0.5	0.0	0.0	0.91(2)
	$R_P = 4.54\%$ $wR_P = 5.84\%$ $R(F^2) = 2.27\%$ $\chi^2 = 3.14$			
	$x = 0.4$ $I4/mcm$ $a = b = 5.777(6)$ Å, $c = 8.187(1)$ Å			
A	0.0	0.5	0.25	0.71(2)
Sn	0.0	0.0	0.0	0.27(3)
O1	0.0	0.0	0.25	0.43(6)
O2	0.2659(2)	0.7659(2)	0.0	1.55(4)
	$R_P = 5.71\%$ $wR_P = 7.2\%$ $R(F^2) = 3.74\%$ $\chi^2 = 5.33$			
	$x = 0.6$ $Imma$ $a = 5.758(3)$ Å, $b = 8.121(5)$ Å, $c = 5.767(6)$ Å			
A	0.0	0.25	0.0025(6)	0.71(2)
Sn	0.0	0.0	0.5	0.78(2)
O1	0.5	0.25	0.0406(4)	1.34(5)
O2	0.25	0.0227(2)	0.75	1.06(2)
	$R_P = 4.35\%$ $wR_P = 5.42\%$ $R(F^2) = 3.79\%$ $\chi^2 = 2.81$			
	$x = 0.8$ $Pbnm$ $a = 5.741(6)$ Å, $b = 5.728(2)$ Å, $c = 8.091(2)$ Å			
A	−0.0000(8)	0.0109(4)	0.25	0.84(2)
Sn	0.0	0.5	0.0	0.08(2)
O1	0.0487(5)	0.4921(7)	0.25	0.95(6)
O2	0.7316(4)	0.2720(4)	0.0301(2)	0.99(3)
	$R_P = 4.41\%$ $wR_P = 5.41\%$ $R(F^2) = 3.10\%$ $\chi^2 = 2.60$			

with falling t, the crystallographically observed average Sn–O distance increases towards the $t = 1$ value. This demonstrates that the true average Sn–O distance is insensitive to t, the local Sn–O–Sn angles decrease smoothly with t, and it is the structural coherence of the bending that changes abruptly at the perovskite phase transitions.

The tilt systems in perovskites are commonly described using Glazer notation, which specifies the rotation of the octahedra about each of the Cartesian axes [15]. The rotations are described by a letter and a superscript. The letter specifies the magnitude of the rotations relative to those about the other Cartesian axes. The superscript indicates whether the rotations in adjacent layers are in phase (+) or out of phase (−); a zero superscript is used when no rotations occur. The alkaline earth stannates undergo the following phase transitions with increasing A cation radius:

$$Pbnm\ (a^+b^-b^-) \rightarrow Imma\ (a^0b^-b^-) \rightarrow I4/mcm\ (a^0a^0c^-) \rightarrow Pm\bar{3}m\ (a^0a^0a^0).$$

This sequence of transitions is also seen at high temperatures in $SrZrO_3$ [11] and in $SrRuO_3$ [16]. The transition from $Pbnm$ to $Imma$ may be continuous in Landau theory because it involves only loss of the in-phase tilting [17]. The transition from $Imma$ to $I4/mcm$ is first order because it involves an abrupt change from a structure with tilts around a diad axis ($a^0b^-b^-$) of the oxygen octahedron to one with the tilts around a tetrad axis ($a^0a^0c^-$). The transition from $I4/mcm$ to $Pm\bar{3}m$ may be continuous in Landau theory.

The cubic $Pm\bar{3}m$ perovskite structure is observed for $0.998 < t < 1.018$, close to the ideal value of tolerance factor $t = 1$ expected for the undistorted structure. The $I4/mcm$

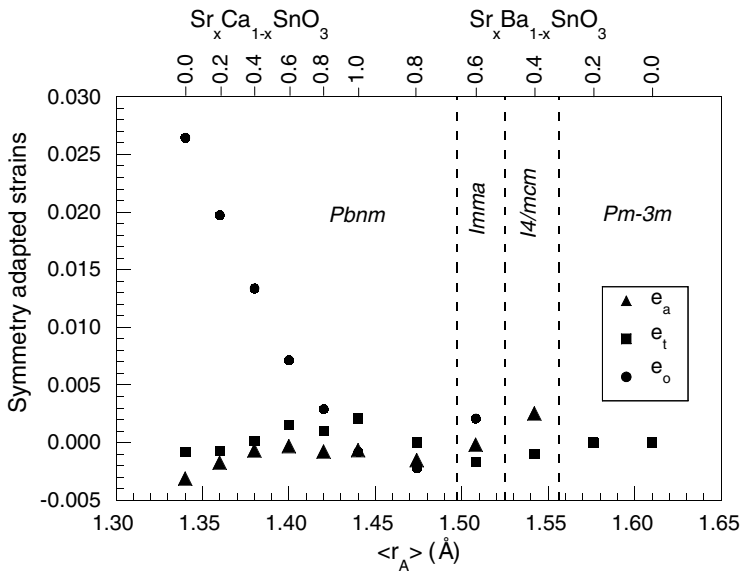

Figure 8. Variation of symmetry-adapted strains with average A cation radius. e_a is the volume strain, e_t is the tetragonal strain and e_o is the orthorhombic strain.

superstructure is a common intermediate between orthorhombic and cubic perovskites. The SnO_6 octahedra in this phase are slightly tetragonally compressed with the axial Sn–O1 bonds 0.002 Å shorter than the equatorial Sn–O2 bonds. This tetragonal compression is consistent with studies on other $I4/mcm$ perovskites [13].

The second orthorhombic phase, with $Imma$ superstructure, is observed at high temperatures in $SrZrO_3$ [11] and $SrRuO_3$ [16] as an intermediate between the $Pbnm$ and $I4/mcm$ phases. The octahedra in this phase are also slightly tetragonally compressed with the axial Sn–O1 bonds 0.002 Å shorter than the equatorial Sn–O2 bonds.

The $Pbnm$ superstructure is very common in perovskites; typical examples are $CaTiO_3$ [13], $SrZrO_3$ [11] and $CaGeO_3$ [18]. It has the largest range of all the space groups in the $ASnO_3$ system, covering the whole $Sr_xCa_{1-x}SnO_3$ series. Strain analysis indicates the orthorhombic strain is dominant in the $Pbnm$ system. This strain decreases as the A cation radius increases. Smith and Welch [6] reported a transition in the $Sr_xCa_{1-x}SnO_3$ system at $x = 0.45$ but we find no evidence for this transition. We observed no peak splitting at the strontium end of the series by eye and determined the space group using superlattice peaks. These superlattice peaks are difficult to observe using x-ray diffraction so the transition observed by Smith and Welch probably corresponds to the disappearance of the visible orthorhombic peak splitting.

As might be expected, the dominant strains are e_t in the $I4/mcm$ phase and e_o in the $Pbnm$ and $Imma$ phases (figure 8). The behaviour of the strains is very similar to that observed in the $Sr_xCa_{1-x}TiO_3$ solid solution, where similar transitions are driven by variations in average A cation radius [14].

Acknowledgments

We thank Alan Hewat at the ILL for help in collecting the neutron powder patterns, and EPSRC for financial support for EHM.

References

[1] Azad A-M, Shyan L L W and Alim M A 1999 *J. Mater. Sci.* **34** 1175–87
[2] Yasuda N, Ohwa H and Asano S 1996 *Japan. J. Appl. Phys.* **35** 5099–103
[3] Shimizu Y, Shimabukuro M, Arai H and Seiyama T 1989 *J. Electrochem. Soc.* **136** 1206–10
[4] Hodjati S, Vaezzadeh S, Petit C, Pitchon V and Kienneman A 2000 *Appl. Catal.* B **26** 5–16
[5] Vegas A, Vallet-Regi M, Gonzalez-Calbet J M and Alario-Franco M A 1989 *Acta Crystallogr.* B **42** 167–72
[6] Smith A J and Welch A J E 1960 *Acta Crystallogr.* **13** 653–6
[7] Green M A, Prassides K, Day P and Neumann D A 2000 *Int. J. Inorg. Mater.* **2** 35–41
[8] Megaw H D 1946 *Proc. Phys. Soc.* **58** 133–52
[9] Andrault D, Itie J P and Farges F 1996 *Am. Mineral.* **81** 822–32
[10] Von Dreele R and Larson A C 1986 GSAS general structure analysis system *Los Alamos National Laboratory Report* LAUR 86-748
[11] Howard C J, Knight K S, Kennedy B J and Kisi E H 2000 *J. Phys.: Condens. Matter* **12** L677–83
[12] Kennedy B J, Howard C J, Thorogood G J and Hester J R 2001 *J. Solid State Chem.* **161** 106–12
[13] Kennedy B J, Howard C J and Chakoumakos B C 1999 *J. Phys.: Condens. Matter* **11** 1479–88
[14] Carpenter M A, Becerro A I and Seifert F 2001 *Am. Mineral.* **86** 348–63
[15] Woodward P M 1997 *Acta Crystallogr.* B **53** 32–43
[16] Kennedy B J, Hunter B A and Hester J R 2002 *Phys. Rev.* B **65** 224103
[17] Howard C J and Stokes H T 1998 *Acta Crystallogr.* B **54** 782–9
[18] Lui X, Wang Y, Liebermann R C, Maniar P D and Navrotsky A 1991 *Phys. Chem. Minerals* **18** 224–30